8314–8324 *Nucleic Acids Research, 2015, Vol. 43, No. 17* *Published online 21 July 2015*
doi: 10.1093/nar/gkv725

In vivo detection and replication studies of α-anomeric lesions of 2′-deoxyribonucleosides

Nicholas J. Amato[1], Qianqian Zhai[1,2], Diana C. Navarro[3], Laura J. Niedernhofer[3] and Yinsheng Wang[1,*]

[1]Department of Chemistry, University of California, Riverside, CA 92521, USA, [2]Department of Chemistry, College of Science, Huazhong Agricultural University, Wuhan, 430070, China and [3]Department of Metabolism and Aging, The Scripps Research Institute Florida, FL 33458, USA

Received May 20, 2015; Revised July 2, 2015; Accepted July 4, 2015

ABSTRACT

DNA damage, arising from endogenous metabolism or exposure to environmental agents, may perturb the transmission of genetic information by blocking DNA replication and/or inducing mutations, which contribute to the development of cancer and likely other human diseases. Hydroxyl radical attack on the C1′, C3′ and C4′ of 2-deoxyribose can give rise to epimeric 2-deoxyribose lesions, for which the *in vivo* occurrence and biological consequences remain largely unexplored. Through independent chemical syntheses of all three epimeric lesions of 2′-deoxyguanosine (dG) and liquid chromatography-tandem mass spectrometry analysis, we demonstrated unambiguously the presence of substantial levels of the α-anomer of dG (α-dG) in calf thymus DNA and in DNA isolated from mouse pancreatic tissues. We further assessed quantitatively the impact of all four α-dN lesions on DNA replication in *Escherichia coli* by employing a shuttle-vector method. We found that, without SOS induction, all α-dN lesions except α-dA strongly blocked DNA replication and, while replication across α-dA was error-free, replicative bypass of α-dC and α-dG yielded mainly C→A and G→A mutations. In addition, SOS induction could lead to markedly elevated bypass efficiencies for the four α-dN lesions, abolished the G→A mutation for α-dG, pronouncedly reduced the C→A mutation for α-dC and triggered T→A mutation for α-dT. The preferential misincorporation of dTMP opposite the α-dNs could be attributed to the unique base-pairing properties of the nucleobases elicited by the inversion of the configuration of the *N*-glycosidic linkage. Our results also revealed that Pol V played a major role in bypassing α-dC, α-dG and α-dT *in vivo*. The abundance of α-dG in mammalian tissue and the impact of the α-dNs on DNA replication demonstrate for the first time the biological significance of this family of DNA lesions.

INTRODUCTION

Aerobic metabolism and exposure to environmental agents produces reactive oxygen species (ROS) endogenously, which can damage DNA and other cellular components (1,2). In addition to generating nucleobase lesions, which may directly impact base-pairing, ROS can damage the 2-deoxyribose moiety in DNA (3,4). Abstraction of a hydrogen atom from 2-deoxyribose gives 2-deoxyribose radicals that can give rise to alkali-labile sites and DNA strand breaks (3,5,6). Studies about the fate of 2-deoxyribose radicals also revealed pathways that compete with the formation of strand breaks (7). One pathway is the chemical repair of the 2-deoxyribose radicals by a hydrogen-atom donor. Improper chemical repair can lead to the inversion of configuration at the C1′, C3′ and C4′ positions, thereby generating the epimeric 2-deoxyribose lesions. For instance, Scheme 1 shows the mechanism for the formation of C1′-epimeric lesions of 2′-deoxynucleosides, i.e. α-2′-deoxynucleosides (α-dNs) (4).

Few studies have been conducted regarding the formation of the C1′-epimeric lesions of α-dNs. The formation of α-2′-deoxyuridine has been unambiguously demonstrated through the independently generated C1′ radical of 2′-deoxyuridine in mononucleoside and in synthetic oligodeoxyribonucleotides (ODNs) (8–10). In addition, it was found that abasic sites and α-2′-deoxyadenosine (α-dA) are the major products when poly(dA), poly(dA-dT) and salmon testis DNA are exposed to γ rays under anaerobic conditions (11). In that study, the identification of α-dN was based on its migration on liquid chromatography (LC) compared to a synthetic standard (11). It is possible that other modified nucleosides may co-elute with α-dA, which may result in an overestimation of the level of α-dA formed in

*To whom correspondence should be addressed. Tel: +1 951 827 2700; Fax: +1 951 827 4713; Email: Yinsheng.Wang@ucr.edu

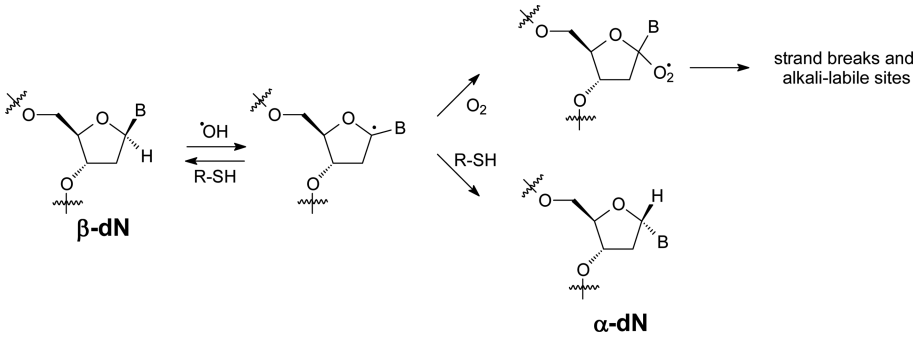

Scheme 1. Formation of α-2′-deoxynucleosides from the improper chemical repair of the C1′-radical by an H-atom donor. 'B' designates nucleobase.

DNA. Moreover, α-dA was not detectable when the aforementioned DNA samples were exposed to γ rays under aerobic conditions (11), leading to further questions about the physiological relevance of these lesions.

The C1′ radical, in addition to forming α-dNs or being converted back to the natural β anomers, can also conjugate with O_2 to yield a peroxyl radical on the C1′, which may ultimately lead to alkali-labile sites and strand breaks in DNA (Scheme 1) (6). The rate constants for the trapping of C1′ radical of dU by β-mercaptoethanol and dithiothreitol in a synthetic duplex ODN is much lower, by ∼1100- and 270-fold, respectively, than that for its conjugation with O_2 (10). This observation, along with the concentration of O_2 in aerated water and the concentration of physiologically relevant thiol, led to the suggestion that the α-anomeric lesions are unlikely a significant family of DNA lesions *in vivo* (10). However, the rates for the C1′ radicals in trapping thiol and in coupling with O_2 may differ for each nucleoside and may also be modulated by packaging of DNA into chromatin. Thus, further understanding of the biological significance of α-dNs necessitates a rigorous assessment about their occurrence *in vivo*.

Unrepaired DNA lesions may confer genomic instability by compromising the fidelity and efficiency of DNA replication and transcription, thereby contributing to the development of cancer and other human diseases, as well as aging (12). The impact of epimeric 2′-deoxyribonucleosides, including the α-dNs, on DNA metabolic processes *in vivo* remains poorly explored, where replication studies were conducted only for α-dA in *Escherichia coli* (13). α-dA was found to moderately block DNA replication in *E. coli* and induce a −1 deletion at the lesion site (13). It remains unclear how other α-dNs perturb DNA replication *in vivo*.

In the present study, we rigorously assessed the formation of one of the α-dNs (α-dG) in mouse pancreatic tissues and investigated the impact of all four α-dNs on the efficiency and fidelity of DNA replication in cells. Our results demonstrated unambiguously the presence of substantial levels of α-dG in mammalian DNA and revealed that the effects of the α-dN lesions on DNA replication depended on the chemical identities of α-nucleosides.

MATERIALS AND METHODS

Materials

All enzymes unless otherwise noted were from New England BioLabs (NEB). Shrimp alkaline phosphatase (SAP) was obtained from Affymetrix, [γ-^{32}P]-ATP was purchased from Perkin-Elmer and acrylamide:bis-acrylamide solution (19:1) and RNase A were obtained from Fisher Scientific. [$^{13}C_{10}$–$^{15}N_2$]-Thymidine was purchased from Cambridge Isotope Laboratories. Nuclease P1, RNase T1, calf intestinal phosphatase (CIP), calf thymus DNA, and phosphodiesterases I and II were obtained from Sigma-Aldrich. All reagents for solid-phase DNA synthesis were purchased from Glen Research and all unmodified ODNs were obtained from Integrated DNA Technologies (IDT). The M13mp7(L2) plasmid and wild-type AB1157 *E. coli* cells were provided by Prof. John M. Essigmann and Prof. Graham C. Walker provided the polymerase-deficient AB1157 cells, which included Δ*pol B1*::spec (Pol II-deficient), Δ*dinB* (Pol IV-deficient), Δ*umuC*::kan (Pol V-deficient) and Δ*dinB* Δ*umuC*::kan (deficient in both Pol IV and Pol V) (14).

Synthesis of [$^{13}C_5$]-α-2′-deoxyguanosine ([$^{13}C_5$]-α-dG)

[$^{13}C_5$]-α-dG was synthesized on a small scale by adapting and optimizing previously reported procedures (Supplementary Scheme S1) (15). Briefly, [$^{13}C_{10}$–$^{15}N_2$]-thymidine (24.7 mg, 0.097 mmol) and anhydrous pyridine (1 ml) were added to a round bottom flask. Acetic anhydride (40 μl, 0.409 mmol) was added to the stirred solution and the reaction was continued at 60°C for 3 h. The solvent was subsequently removed using a rotary evaporator and the remaining residue was dried under vacuum overnight.

A portion of the resulting crude 3′,5′-di-*O*-acetyl-[$^{13}C_{10}$–$^{15}N_2$]-thymidine (5.0 mg, 0.020 mmol) was dissolved in ethyl acetate and transferred to a 15 ml flask. The solvent was removed using a rotary evaporator and the solid residue dried under vacuum for 30 min. N^2-isobutyrylguanine (9.0 mg, 0.041 mmol), prepared as previously described (16), was added to the mixture. Anhydrous acetonitrile (1 ml) was subsequently added and the solution was stirred at room temperature for 10 min. Bis(trimethylsilyl)acetamide (20 μl, 0.070 mmol) was then added to the mixture. After stirring at 70°C for 15 min, trimethylsilyl trifluoromethanesulfonate (4 μl, 0.020 mmol) was added and the reaction was continued at 70°C for 4 h. The reaction mixture was cooled to

room temperature, the solvent was removed and the solid residue dried under vacuum. The resulting crude 3′,5′-di-*O*-acetyl-N^2-isobutyryl-[$^{13}C_5$]-2′-deoxyguanosine was purged with nitrogen for 30 min, 2 M ammonia in methanol (4 ml) was added and the reaction was continued at 40°C for 12 h. Ammonium hydroxide solution (30%, 4 ml) was then added and the reaction mixture was stirred at 40°C for 36 h. The solvent was removed under reduced pressure and the desired [$^{13}C_5$]-α-dG was purified from the reaction mixture using High-performance liquid chromatography (HPLC), where an Agilent 1200 series HPLC and a Grace Alltima reversed phase column (5 μm HP C18, 4.6 × 250 mm) were employed. The yield for the synthesis of [$^{13}C_5$]-α-dG was estimated to be 30% based on HPLC analysis. The identity of [$^{13}C_5$]-α-dG was confirmed by LC-MS/MS analysis (Supplementary Figure S1).

Synthesis of [$^{13}C_5$]-2′-deoxy-β-D-xyloguanosine ([$^{13}C_5$]-xylo-dG)

The isotope-labeled xylo-dG was synthesized at a small scale using procedures adapted and optimized from those reported previously (Supplementary Scheme S2) (15,17,18). Briefly, [$^{13}C_{10}$–$^{15}N_2$]-thymidine (20.0 mg, 0.079 mmol) in a 50-ml round-bottom flask was purged with nitrogen for 30 min. Anhydrous pyridine (3.75 ml) was added to the stirred solution followed by addition of 4,4′-dimethoxytrityl chloride (32 mg, 0.094 mmol). After stirring at room temperature for 3 h, methanol (4 ml) was added and the solution was stirred for another 30 min. The solvent was removed by rotary evaporation. The crude residue was dissolved in 10 ml CH_2Cl_2 containing 0.1% triethylamine (TEA), washed three times each with saturated sodium bicarbonate (10 ml) and doubly distilled water (ddH_2O, 10 ml), and dried with anhydrous $MgSO_4$. The 5′-*O*-DMTr-[$^{13}C_5$–$^{15}N_2$]-thymidine was purified by silica gel column chromatography (35% yield).

The purified 5′-*O*-DMTr-[$^{13}C_5$–$^{15}N_2$]-thymidine (15 mg, 0.027 mmol) was co-evaporated with anhydrous toluene in a flask and purged with nitrogen for 30 min. The resulting material was dissolved in 0.5 ml of anhydrous pyridine and the solution was stirred for 10 min. The reaction mixture was subsequently cooled in an ice-bath. Mesyl chloride (10 μl, 0.129 mmol) was then added and the reaction was stirred at 0°C for 3 h. The reaction was quenched by ddH_2O (0.5 ml) and the solvent removed by rotary evaporation. The resulting residue was dissolved in 0.5 ml CH_2Cl_2 containing 0.1% TEA, washed three times with equal volumes of ddH_2O and the solvent removed by rotary evaporation.

The resulting crude 5′-*O*-DMTr-3′-*O*-mesyl-[$^{13}C_5$–$^{15}N_2$]-thymidine (17.12 mg, 0.027 mmol) was dissolved in ethanol (1 ml) and the mixture stirred at 40°C to completely dissolve the starting material. ddH_2O (0.54 ml) was added to the solution and the mixture was cooled to room temperature. This was followed by drop-wise addition of 0.1 ml of 1.0 M NaOH solution. The reaction was stirred at room temperature overnight. Additional NaOH solution (1 M, 0.2 ml) was added drop-wise and the reaction mixture was heated to 95°C. After maintaining the reaction at 95°C for 5 h, the mixture was cooled to room temperature. The solvent was removed by rotary evaporation. The dried residue was dissolved in 10 ml CH_2Cl_2 containing 0.1% TEA, washed with an equal volume of ddH_2O three times and the solvent removed under reduced pressure.

The crude 5′-*O*-DMTr-[$^{13}C_5$–$^{15}N_2$]-xylothymidine (15.01 mg, 0.027 mmol) was dissolved in 80% glacial acetic acid (3 ml) and refluxed at 120°C for 10 min. The reaction was allowed to cool and the solvent evaporated. The resulting residue was dissolved in an equal-volume mixture of ddH_2O and chloroform. The aqueous layer was isolated, washed with chloroform three times and dried to yield the [$^{13}C_{10}$–$^{15}N_2$]-xylothymidine (73% yield, 5 mg, 0.021 mmol). The [$^{13}C_{10}$–$^{15}N_2$]-xylothymidine was then employed to synthesize [$^{13}C_5$]-xylo-dG following the aforementioned method for preparation of [$^{13}C_5$]-α-dG. The resulting [$^{13}C_5$]-xylo-dG was purified by HPLC and characterized by LC-MS/MS (Supplementary Figure S3), as described for [$^{13}C_5$]-α-dG. The unlabeled xylo-dG used for LC-MS/MS confirmation was also synthesized following these procedures and confirmed by ^{1}H-NMR analysis (Supplementary Figure S2).

Synthesis of 2′-deoxy-β-*L-threo*-guanosine (threo-dG)

4′-Phenylseleno-*L-threo*-thymidine (73.11 mg, 0.183 mmol), synthesized following published procedures (Supplementary Scheme S3) (19), was purged with nitrogen for 30 min and dissolved in anhydrous pyridine (1.25 ml). Acetic anhydride (0.075 ml, 0.77 mmol) was subsequently added and the reaction was refluxed at 60°C for 3 h. The solvent was evaporated and the desired 3′,5′-di-*O*-acetyl-4′-phenylseleno-*L-threo*-thymidine was purified from the reaction mixture by silica gel column chromatography (68% yield, 60 mg, 0.124 mmol).

The purified 3′,5′-di-*O*-acetyl-4′-phenylseleno-*L-threo*-thymidine (30 mg, 0.062 mmol), thiophenol (0.636 ml, 6.22 mmol) and toluene (2.47 ml) were added to a 10 ml Pyrex tube. The solution was bubbled with nitrogen for 30 min and then irradiated on ice with a medium-pressure mercury lamp. After 3 h of UV irradiation, thin-layer chromatography (TLC) analysis revealed the consumption of the majority of the starting material. The solvent was removed and the crude product purified using silica gel column chromatography to remove the thiophenol and the remaining starting material. The two diastereomers, i.e. 3′,5′-di-*O*-acetyl-*L-threo*-thymidine and 3′,5′-di-*O*-acetyl-thymidine, which were previously shown to be formed from photochemically generated C4′ radical (20), were purified by HPLC and their structures confirmed by ^{1}H-NMR analyses (Supplementary Figure S4). The desired 2′-deoxy-β-*L-threo*-guanosine was synthesized from 3′,5′-di-*O*-acetyl-*L-threo*-thymidine using the transglycosylation procedures described above for the preparation of [$^{13}C_5$]-α-dG (Supplementary Scheme S3). The resulting 2′-deoxy-β-L-*threo*-guanosine was purified from the reaction mixture by HPLC and characterized by LC-MS/MS and nuclear magnetic resonance (NMR) analyses (Supplementary Figures S5 and S6).

Extraction of DNA from mouse pancreatic tissues

Mouse tissues were obtained in accordance with the guidelines of The Scripps Research Institute Florida Institutional

Animal Care and Use Committee. Mouse pancreatic tissues (50 mg) were grounded into fine powders in the presence of liquid nitrogen. The powders were dispersed in 50 μl of lysis buffer [400 mM NaCl, 20 mM Tris, 20 mM ethylenediaminetetraacetic acid, 1% (w/v) sodium dodecyl sulphate, pH 8.0] and digested with proteinase K (10 U) at 55°C overnight. Saturated NaCl solution (25 μl) was added and the mixture was incubated at 55°C for 15 min. The mixture was centrifuged at 12 000 *g* and 4°C for 30 min. To the supernatant were added two volumes of cold ethanol and the solution was placed at −20°C overnight. The precipitated DNA was isolated by centrifugation at 12 000 *g* for 10 min at 4°C. Residual RNA was removed by an overnight digestion at 37°C with RNase A (2.5 μl, 30 mg/ml) and RNase T1 (62.5 U). The enzymes were removed by chloroform extraction and the DNA was desalted by ethanol precipitation.

Enzymatic digestion of DNA

The mouse pancreatic DNA (25 μg) and calf thymus DNA (25 μg) were separately digested at 37°C for 48 h with nuclease P1 (1 U) and phosphodiesterase II (0.001 U) in a 150-μl buffer containing 30 mM NaOAc (pH 5.6), 10 mM $ZnCl_2$ and 0.04 mM *erythro*-9-(2-hydroxy-3-nonyl)adenine (EHNA). Alkaline phosphatase (10 U), phosphodiesterase I (0.02 U), 20 μl Tris–HCl (0.5 M, pH 8.9) and 27 μl ddH_2O were added to the digestion mixture. After incubation at 37°C for 2 h, 9.5 μl of 1 M formic acid was added to quench the reaction. [$^{13}C_5$]-α-dG (250 fmol) and [$^{13}C_5$]-xylo-dG (1 pmol) were then added. The enzymes were removed by chloroform extraction and the resulting aqueous layer was dried in a Speed-vac.

To evaluate the digestion efficiency of DNA containing modified α-dNs, we digested the 12mer α-dG-containing ODN (5 nmol) following the above-described enzymatic digestion procedures and subjected the resulting nucleoside mixture to HPLC analysis (Supplementary Figure S15). The molar ratios of dG, dC and dT to α-dG were determined to be 3.7, 2.2 and 3.1, respectively, which were in good agreement with the expected ratios of 4.0, 2.0 and 3.0, respectively, thereby supporting that the enzymatic digestion procedures facilitated the nearly quantitative release of α-dG from DNA. In this respect, we did not determine the molar ratio of dA over α-dG because dA is partially deaminated to 2′-deoxyinosine (Supplementary Figure S7).

HPLC enrichment

An Agilent 1200 series HPLC and a Grace Alltima HP C18 reversed-phase column (4.6 × 250 mm, 5 μm in particle size) were used for the enrichment of α-dG from the nucleoside mixture. The mobile phases were 10 mM ammonium formate (solution A) and methanol (solution B) and the flow rate was 1 ml/min. The following gradient was employed: 42 min at 1% B, 1 min 1–2% B, 17 min at 2% B, 1 min 2–5% B and 9 min 5% B. Fractions from three retention time windows (32.0–33.5, 33.5–35.0 and 35.0–36.5 min) were collected, dried in a Speed-vac and stored in a −20°C freezer, where the collection window for the target α-dG was established using the α- and β-dN standards (Supplementary Figures S8 and S9).

LC-MS/MS analysis of α-dG

The enriched fractions were dissolved in 10 μl ddH_2O and 7.5 μl was used for LC-MS/MS analysis (Figure 2 and Supplementary Figure S10). An Agilent 1200 capillary HPLC pump (Agilent Technologies) and a 0.5 × 250 mm Zorbax SB-C18 column (5 μm in particle size, Agilent) were used for the separation. The mobile phases were 0.1% formic acid in ddH_2O (solution A) and 0.1% formic acid in methanol (solution B). The flow rate was 8.0 μl/min and the gradient consisted of 5 min 0–3% B, 14 min 3–10% B, 1 min 10–70% B and 5 min 70% B. The eluent was directed to an LTQ linear ion trap mass spectrometer (Thermo Electron, San Jose, CA, USA), where the fragmentations of the $[M+H]^+$ ions of α-dG (*m*/*z* 268) and [$^{13}C_5$]-α-dG (*m*/*z* 273) were monitored. The levels of α-dG were quantified by using the constructed calibration curve for α-dG (Supplementary Figure S11).

Syntheses of α-dN phosphoramidites and automated solid-phase DNA synthesis

All four α-2′-deoxyribonucleosides were purchased from ChemGenes (Willington, MA, USA). The phosphoramidite building blocks for the α-dNs were prepared as previously described (21). Automated solid-phase DNA synthesis was performed using a Beckman Oligo 1000S DNA Synthesizer following standard procedures. The sequence of the synthesized ODNs was 5′-ATGGCGXGCTAT-3′, where 'X' indicates the α-dNs.

Deprotection, HPLC separation and mass spectrometric characterizations of the 12mer α-dN-harboring ODNs

The α-dN-containing ODNs were cleaved from the solid support resin and deprotected by incubating the resin in 1 ml of 30% ammonium hydroxide solution at 55°C for 16 h. The resulting solution was dried in a Speed-vac and the solid residue was reconstituted in water and purified by HPLC. A Kenetex XB-C18 Column (5 μm in particle size, 100 Å in pore size, 4.6 × 250 mm, Phenomenex) was used and the mobile phases consisted of 50 mM triethylammonium acetate (TEAA, solution A) and 30% CH_3CN in 50 mM TEAA (solution B). The purified ODNs were further desalted using an Aeris Widepore XB-C18 column (3.6 μm in particle size, 100 Å in pore size, 4.6 × 150 mm, Phenomenex), where the mobile phases were water (solution A) and methanol (solution B). The purified ODNs were then characterized by ESI-MS and MS/MS analyses (Supplementary Figures S12–S15).

Preparation of lesion-bearing 22mer ODNs

The purified 12mer α-dN-containing ODNs were phosphorylated using T4 polynucleotide kinase. The phosphorylated α-dN-bearing ODNs were individually ligated to a 10mer ODN (5′-AGTGGAAGAC-3′) with T4 DNA ligase in the presence of a 26mer complementary strand in the ligase buffer at 16°C overnight. The resulting 22mer lesion-bearing ODNs were purified by denaturing polyacrylamide gel electrophoresis (PAGE).

Construction of single-stranded lesion-containing and lesion-free competitor genomes

The single-stranded α-dN-containing and lesion-free competitor M13mp7(L2) genomes were prepared according to previously established procedures (22). Briefly, 20 pmol of the M13 genome was digested with EcoRI (40 U) to linearize the genome. The resulting vector was annealed with two scaffolds (5′-CTTCCACTCACTGAATCATGGTCATAGCTTTC-3′ and 5′-AAAACGACGGCCAGTGAATTATAGC-3′, 25 pmol each). The 5′-phosphorylated 22mer lesion-bearing ODN (30 pmol) was added to the mixture and ligated to the M13 vector at 16°C overnight using T4 DNA ligase (800 U). The remaining un-ligated, linear DNA was removed by treating with T4 DNA polymerase (20 U), which has 3′ → 5′ exonuclease activity, at 16°C for 1 h. The circular lesion-containing M13 vectors were purified using a Cycle Pure Kit (Omega). The concentration of each of the lesion-containing genomes was normalized to the lesion-free competitor genome as previously described (22).

Transformation of lesion-containing and lesion-free competitor genomes into *E. coli* cells

The lesion/competitor genome ratios were 2:1 for α-dA and α-dT, and 5:1 for α-dG and α-dC for replication experiments in wild-type AB1157 *E. coli* cells without SOS induction. For replication experiments in SOS-induced cells, the molar ratios of the lesion/competitor genomes were 2:1, with the amount of the competitor genome being 25 fmol for all experiments. Transformation and SOS induction were conducted according to previously reported procedures (14,22,23). Immediately following transformation, the *E. coli* cells were grown in Luria Broth media at 37°C for 6 h. The phage containing the progeny genome was isolated and amplified in SCS110 *E. coli* cells. Finally, the progeny genome was purified using the QIAprep Spin M13 kit (Qiagen) and quantified using UV absorption measurements.

Quantification of bypass efficiencies and mutation frequencies

A modified version of the competitive replication and adduct bypass (CRAB) assay (22,24,25) was employed to quantify the bypass efficiencies and mutation frequencies of the α-dNs (Figure 3). Polymerase chain reaction (PCR) amplification of the desired region of the M13 progeny genome was carried out using Phusion high-fidelity DNA polymerase. The PCR primers were 5′-YCAGCTATGACCATGATTCAGTGAGTGGA-3′ and 5′ -YTCGGTGCGGGCCTCTTCGCTATTAC-3′ (Y = 5′-amino-modifer-C6). The PCR amplification consisted of four cycles: cycle 1 (1×): 98°C (30 s); cycle 2 (30×): 98°C (10 s), 65°C (30 s), 72°C (15 s); cycle 3 (1×): 72°C (5 min); cycle 4 (1×): 4°C (50 s). All PCR products were purified using the Cycle Pure Kit. The resulting PCR products were subjected to a series of enzymatic digestions and labeling for PAGE analysis to determine the bypass efficiency (BPE) and mutation frequency, as previously described (23). Briefly, 50 ng of PCR product was digested with BbSI (10 U) and dephosphorylated using SAP (1 U) in 10 μl of CutSmart^{TM} buffer at 37°C for 1 h. The SAP was deactivated by heating at 65°C for 7 min. [γ-^{32}P]ATP and T4 polynucleotide kinase (T4 PNK, 10 U) were added to the resulting mixture and incubated at 37°C for 1 h to label the restriction fragments. T4 PNK was deactivated by heating at 75°C for 20 min. Finally, the reaction mixture was digested with MluCI (10 U) at 37°C for 30 min and quenched with 15 μl formamide gel loading buffer (2×) containing xylene cyanol FF and bromophenol blue loading dyes. The DNA digestion mixtures were then resolved on a 30% native PAGE (acrylamide:bis-acrylamide = 19:1) and band intensities were quantified using a Typhoon 9410 Variable Mode Imager. The enzymatic digestions led to the release of a short duplex consisting of d(^{32}P-GGCGMGCTAT)/d(AATTATAGCN), where 'M' and 'N' designate the nucleobase incorporated at the lesion site and its complementary base in the opposite strand, respectively, as a result of DNA replication *in vivo*. We found that, on native PAGE, the restriction fragment corresponding to the putative −1 deletion product, d(^{32}P-GGCGGCTAT), could not be separated from the restriction fragment emanating from the error-free replication of the dA- or α-dA-containing genome, i.e. d(^{32}P-GGCGAGCTAT). Likewise, we were not able to resolve the restriction products with a C or T at the initial lesion site, i.e. d(^{32}P-GGCGCGCTAT) and d(^{32}P-GGCGTGCTAT). Thus, we reversed the order of digestion for the two restriction enzymes, which allowed for the radiolabeling of the complementary strand and facilitated the differentiation of the above products by native PAGE analysis, as previously described (23,26). The impact of the α-dN lesions on replication fidelity is represented by the mutation frequency (i.e. the percent of mutant restriction fragments in the total amount of restriction fragments (mutant and non-mutated) generated from the PCR products of the lesion-carrying progeny genome). To evaluate the efficiency of *in vivo* replication of the lesion-carrying genome, the BPE was calculated using the following formula:

$$\mathrm{BPE}(\%) = \frac{(\text{Lesion Signal})/(\text{Competitor Signal})}{(\text{Control Signal})/(\text{Competitor Signal})} \times 100\%$$

Identification of mutant products by LC-MS/MS

A large amount (1–3 μg) of PCR products were also digested with BbSI (50 U) in the presence of SAP (20 U) in 100 μl of CutSmart^{TM} buffer at 37°C for 2 h. The SAP was deactivated by heating at 65°C for 7 min. MluCI (50 U) was subsequently added to the digestion mixture and the mixture was heated at 37°C for 1 h. The enzymes were then removed by extraction with phenol/chloroform/isoamyl alcohol (25:25:1, v/v). The aqueous layer was desalted using HPLC. The resulting ODN mixture was dried, reconstituted in ddH_2O and subjected to LC-MS/MS analysis on an LTQ linear ion trap mass spectrometer. An Agilent Zorbax SB-C18 column (0.5 × 250 mm, 5 μm in particle size) was used. The mobile phases were 400 mM HFIP (pH 7.2, solution A) and methanol (solution B) and the gradient was 5–20% B in 5 min and 20–50% B in 30 min. After each

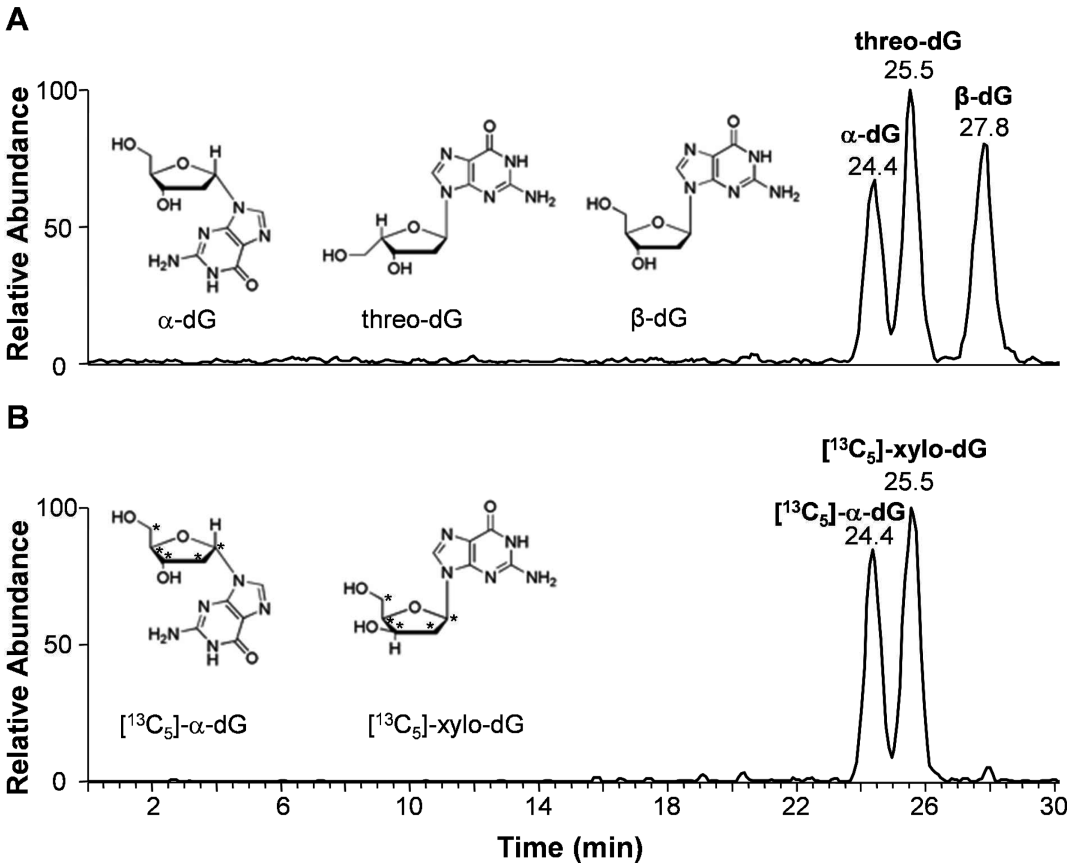

Figure 1. LC-MS/MS analysis of all four epimers of dG utilizing optimized LC conditions. (**A**) The selected-ion chromatogram (SIC) for the m/z 268→152 transition, which monitors the loss of a 2-deoxyribose and the result illustrated the separation of the unlabeled α-dG, threo-dG and β-dG from each other. (**B**) The SIC for the m/z 273→152 transition, which monitors the loss of a [$^{13}C_5$]-2-deoxyribose from [$^{13}C_5$]-α-dG and [$^{13}C_5$]-xylo-dG and the result supported the separation of [$^{13}C_5$]-α-dG and [$^{13}C_5$]-xylo-dG. Co-elution of xylo-dG and threo-dG is demonstrated by utilizing unlabeled threo-dG and labeled [$^{13}C_5$]-xylo-dG, which both elute at 25.5 min. The '*' indicates the presence of ^{13}C atoms.

sample analysis, the column was washed with 90% B for 10 min and a blank run was added to avoid sample carryover. The ion-transport tube for the mass spectrometer was maintained at 300°C, the collision energy was 35 and the activation Q was 0.25. The $[M\text{-}3H]^{3-}$ of d(GGCGMGCTAT) (M = A, T, G or C) and d(AATTATAGCN) (N = A, T, G or C), which were derived from the strand initially containing the α-dNs and the complementary strand, respectively, were monitored in MS/MS. Additionally, the MS/MS of the $[M\text{-}3H]^{3-}$ ions of d(GGCGGCTAT) and d(AATTATAGC) were monitored to confirm the absence of −1 deletion at the lesion site. The fragment ions observed in MS/MS were manually assigned.

RESULTS AND DISCUSSION

Detection of α-dG in DNA isolated from mammalian tissues and in calf thymus DNA

Our long-term goal is to understand the biological significance of the α-dN lesions. To this end, we set out to first rigorously assess the amount of the α-dN lesions in mammalian tissue DNA. We began with the chemical syntheses of all three epimeric 2-deoxyribose lesions of dG and employed them as standards to determine, by using LC-MS/MS analysis, if α-dG accumulates in mammalian tissues to appreciable levels. It is important to emphasize that, owing to the structural similarity among the three epimeric 2-deoxyribose lesions of dG and the canonical dG, it is challenging to reliably measure the level of α-dG in DNA without interference of the other two epimeric 2-deoxyribose lesions and the natural nucleoside dG. By utilizing optimized LC conditions for LC-MS/MS analysis, we were able to resolve α-dG from the other three dG derivatives, which enabled the reliable quantification of α-dG (Figure 1). We were also able to separate the C3′ and C4′ epimers of dG from β-dG, although we were unable to resolve the C3′ and C4′ epimers of dG from each other (Figure 1). With the optimized LC-MS/MS conditions and the stable isotope-labeled α-dG as an internal standard, we were able to quantify the levels of α-dG in mammalian DNA. α-dG was present at levels of 2.2–2.7 lesions per 10^6 nucleosides in mouse pancreatic tissues. No significant difference in adduct levels was observed between animals at 5 months and 2.5 years of age (Figure 2), indicating that α-dG does not appear to accumulate with age. For comparison, we also measured the levels of the (5′*S*) diastereomer of 8,5′-cyclo-2′-deoxyguanosine (*S*-cdG), an oxidatively induced DNA lesion arising from the C5′ radical of 2-deoxyribose (27),

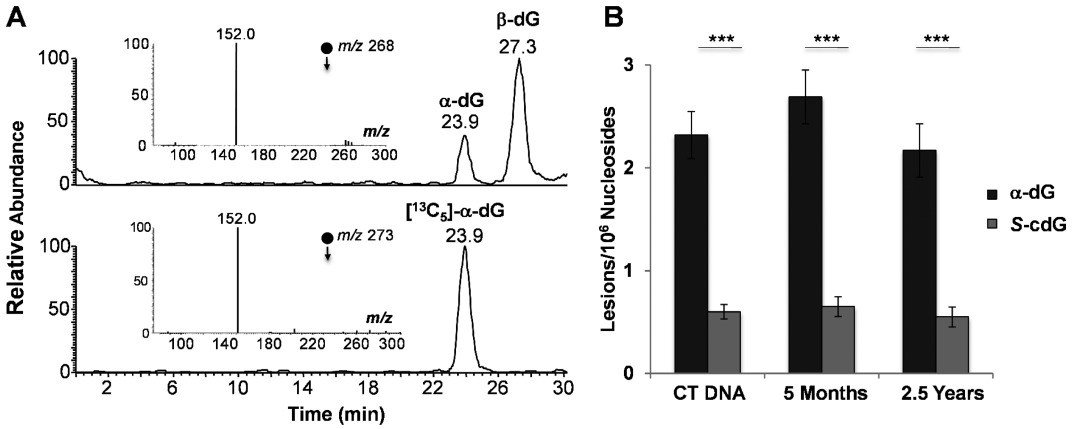

Figure 2. Quantification of α-dG and *S*-cdG in calf thymus (CT) DNA and in DNA isolated from mouse pancreatic tissues by using LC-MS/MS with the stable isotope-dilution method. (**A**) Representative LC-MS/MS results for the detection of α-dG enriched from the nucleoside mixture of DNA isolated from mouse pancreatic tissue. Shown are the selected-ion chromatograms (SICs) for monitoring the neutral loss of a 2-deoxyribose from the $[M+H]^+$ ions of unlabeled α-dG (m/z 268→152) and [$^{13}C_5$]-α-dG (m/z 273→152). Depicted in the insets are the MS/MS averaged from the 23.9 min peak observed in the SICs. (**B**) The levels of α-dG and *S*-cdG in calf thymus DNA (CT DNA) and in DNA isolated from the pancreatic tissues of young (5 months) and old (2.5 years) mice. The data represent the mean and standard deviation of results obtained from the analyses of tissue samples of three different mice in each group. The level of *S*-cdG in CT DNA was based on our previously reported results (32). $*P < 0.05$; $**P < 0.01$; and $***P < 0.001$. The *P*-values were calculated using unpaired Student's *t*-test.

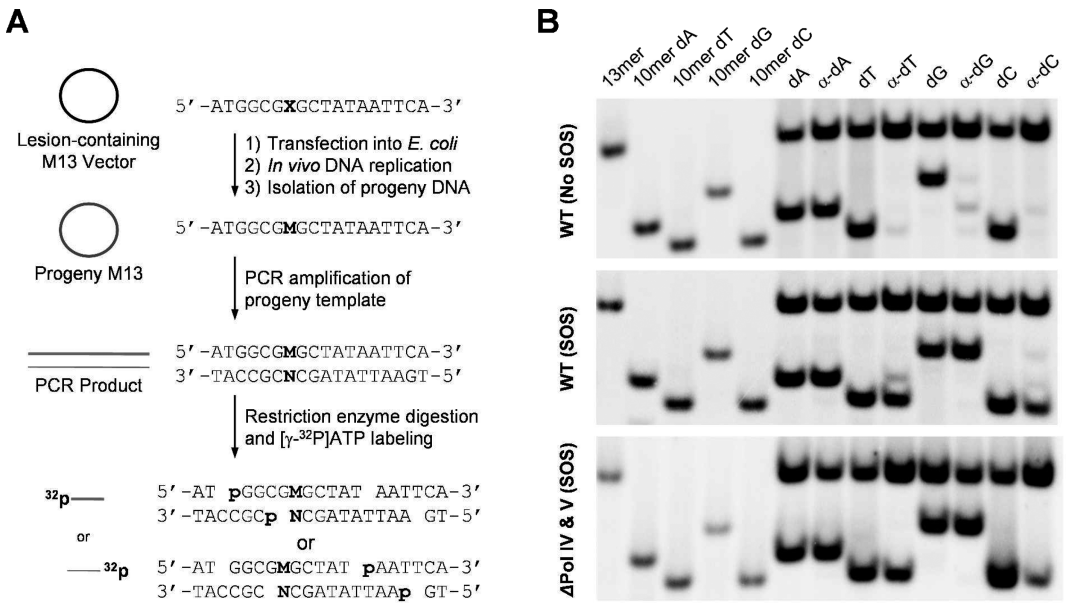

Figure 3. *In vivo* replication, restriction enzyme digestions, labeling and PAGE analysis for determining the bypass efficiencies and mutation frequencies of the α-dN lesions in *Escherichia coli* cells. (**A**) A scheme illustrating the experimental procedures. Not shown is the lesion-free M13 competitor genome, which is co-transfected with the control or lesion-containing M13 genome. Restriction digestion of the PCR products of the progeny for the lesion-free competitor genome yields a 13mer sequence, with M = ATAA and N = TATT. (**B**) Representative PAGE analyses with labeling of the original strand d(GGCGMGCTAT), where 'M' indicates the nucleobase incorporated at the site of the lesion as a result of DNA replication *in vivo*. '13mer', '10mer dA', '10mer dT', '10mer dG' and '10mer dC' designate standard synthetic ODNs of d(GGCGMGCTAT), where 'M' represents ATAA, A, T, G and C, respectively.

in the same tissues using our previously established method (28). The levels of α-dG were significantly higher than those of *S*-cdG (Figure 2). We also measured the level of α-dG in commercially available calf thymus DNA and our results showed that the level is comparable as what we found in mouse pancreatic tissues and is again substantially higher than the level of *S*-cdG (Figure 2). Together, these results indicate that α-dG levels *in vivo* are on the same order of magnitude as other endogenous oxidative lesions that contribute to human disease.

Replication blockage effects of α-dN lesions *in vivo*

A previous study demonstrated that α-dA stalls DNA replication in *E. coli*, giving a BPE of ∼20% relative to dA (13). The effect of other α-dNs on DNA replication was, however, not examined. We decided to systematically assess how

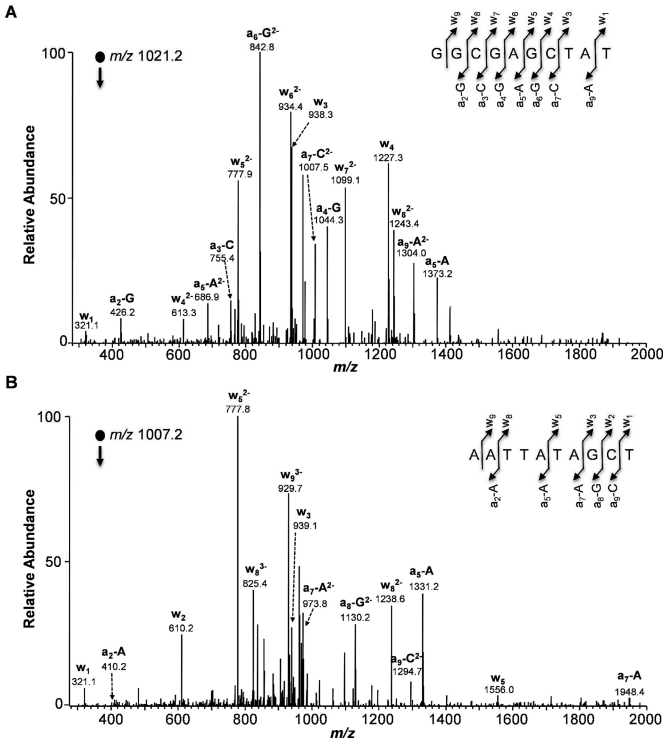

Figure 4. Representative LC-MS/MS analysis of mutagenic products generated during the replicative bypass of the α-dN lesions in *Escherichia coli* cells. (**A**) ESI-MS/MS for the identification of G→A mutations arising from the replication of α-dG-containing M13 genome in wild-type AB1157 cells without SOS induction. Shown is the MS/MS of the $[M-3H]^{3-}$ ion of d(GGCGAGCTAT). (**B**) ESI-MS/MS for the identification of T→A mutations emanating from the replication of α-dT-containing M13 genome in Pol II-deficient AB1157 cells with SOS induction. Shown is the MS/MS of the $[M-3H]^{3-}$ ion of d(AATTATAGCT).

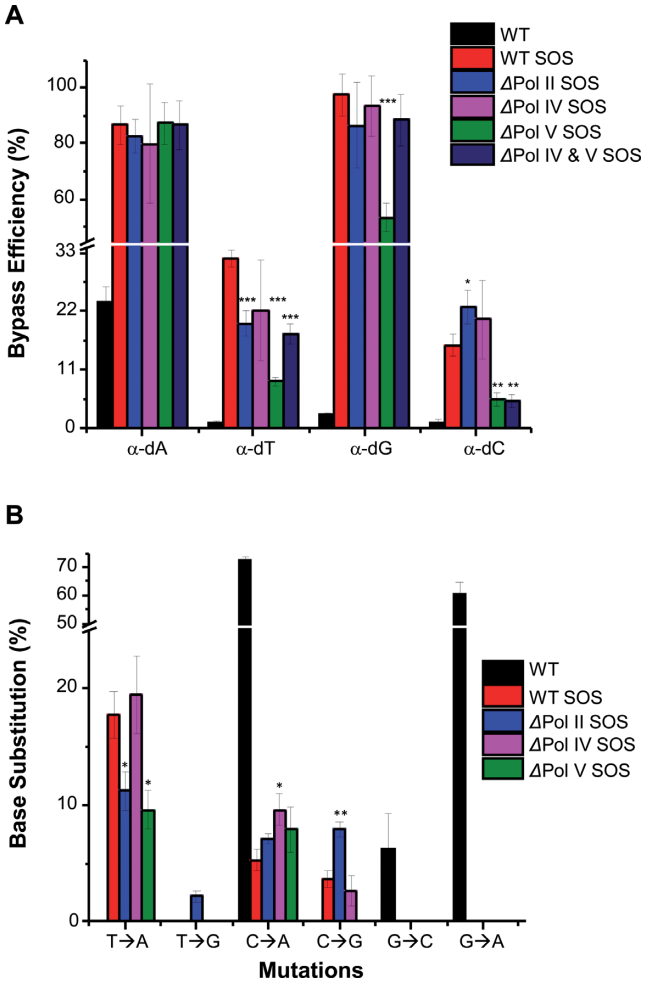

Figure 5. Replication bypass efficiencies (**A**) and mutation frequencies (**B**) of the α-dN lesions in *Escherichia coli* cells. Replication experiments were conducted in wild-type AB1157 *E. coli* cells proficient in all three TLS polymerases in the absence or presence of SOS induction, as well as in SOS-induced AB1157 cells deficient in Pol II, Pol IV, Pol V, or both Pol IV and Pol V. T→A, T→G, C→A, C→G, G→C and G→A mutations were identified, and no mutations were observed when neither Pol IV nor Pol V was present. The data represent the mean and standard deviation of results obtained from three parallel replication experiments. $*P < 0.05$; $**P < 0.01$; and $***P < 0.001$. The *P*-values were calculated using unpaired Student's *t*-test.

the four α-dNs perturb the efficiencies and fidelities of DNA replication in cells. To this end, we employed a modified version of the CRAB assay (25) to determine the BPE and mutation frequency of the four α-dNs in isogenic AB1157 *E. coli* cells that are proficient or deficient in one or more of the SOS-induced DNA polymerases. In this assay, the lesion-containing and lesion-free competitor genomes are mixed at a fixed molar ratio and allowed to replicate in *E. coli* cells. The progeny genomes are then isolated, amplified by PCR and the PCR products are digested by restriction enzymes so that the restriction fragments containing the initial damage site can be analyzed by PAGE and LC-MS/MS to identify the mutant products arising from *in vivo* replication and to quantify the BPEs and mutation frequencies (Figures 3 and 4, and Supplementary Figures S16–S18).

Our results revealed a 24% BPE for α-dA in wild-type AB1157 cells, which is similar to the previous data (13). α-dT, α-dG and α-dC, on the other hand, exhibited markedly lower BPEs (1–3%, Figure 5A). Thus, the replication blockage effect is highly dependent upon the chemical identities of the α-dNs.

We next examined if SOS induction and the ensuing increased expression of translesion synthesis (TLS) DNA polymerases can promote the replicative bypass of the α-dN lesions in AB1157 *E. coli* cells. Upon SOS induction, the BPEs for all four α-dNs were significantly elevated, with the two α-purine nucleosides (α-dA and α-dG) being more efficiently bypassed than the two α-pyrimidine counterparts (α-dC and α-dT, Figure 5A).

We also conducted the replication experiments in SOS-induced *E. coli* cells that are deficient in Pol II, Pol IV, Pol V or both Pol IV and Pol V. The absence of Pol IV did not affect the BPE for any of the α-dNs. On the other hand, depletion of Pol V led to a significant decrease in BPE for all of the α-dNs except for α-dA. Removal of Pol II led to a significant drop in BPE for α-dT, but not for any other α-dNs. Depletion of Pol IV in the Pol V-deficient background led to increased BPEs for α-dG and α-dT, but not α-dA (Figure 5A). Thus, the BPEs of the α-dNs are dictated by

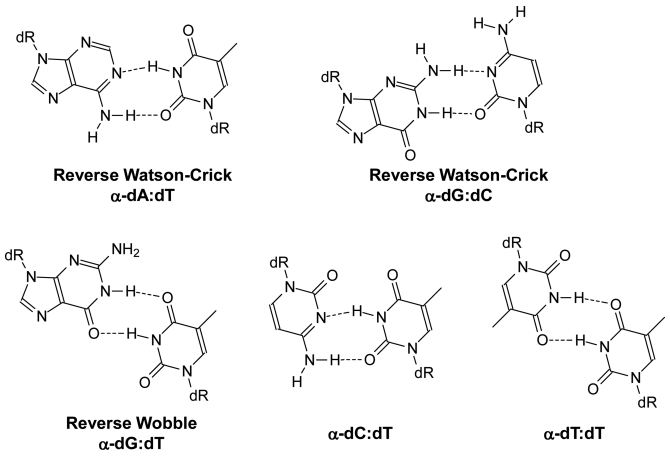

Scheme 2. Proposed base-pairings involved in correct nucleotide incorporations opposite α-dA and α-dG, along with the misinsertion of dTMP opposite α-dC, α-dG and α-dT. 'dR' designates 2-deoxyribose.

both the chemical nature of the modified nucleosides and the availability of TLS polymerases.

Mutagenic properties of α-dN lesions

We next determined the mutagenic properties of the α-dNs during replication in SOS-induced *E. coli* cells that are proficient or deficient in TLS polymerases (Figure 5B). We identified the mutant products by LC-MS/MS and PAGE analyses of restriction fragments of PCR products from progeny genomes (Figures 3 and 4 and Supplementary Figures S16–S18) and quantified the mutation frequencies based on PAGE analysis of these restriction fragments (Figure 5B). In wild-type AB1157 cells without SOS induction, both α-dC and α-dG directed dTMP insertion, as reflected by 72% of C→A mutation and 60% of G→A mutation for α-dC and α-dG, respectively. A low frequency of G→C mutation was also observed for α-dG (6%). SOS induction led to complete abrogation (i.e. G→A transition and G→C transversion) or marked reduction (i.e. C→A transversion) in these mutations. These reductions in mutation frequency were accompanied by elevated BPEs for the two lesions, suggesting that the increased levels of TLS polymerases induced by the SOS response promote efficient and accurate bypass of α-dC and α-dG *in vivo*. On the other hand, SOS induction led to T→A and C→G mutations for α-dT and α-dC, respectively, which were not observed in un-induced wild-type AB1157 cells.

With respect to α-dA, no mutations were observed in the presence or absence of SOS induction. One-nucleotide deletion (−1 deletion) at the α-dA site was observed in a previous study (13). The prevalence of this deletion was found to be modulated by the 3′-neighboring nucleoside of α-dA, where the frequencies of this mutation were 26 and 1% with the 3′-vicinal nucleosides being dT and dG, respectively (13). Thus, the lack of −1 deletion in our study might be attributed to the fact that the 3′-neighboring nucleoside is a dG. Because the focus of the present study was placed on understanding the impact of all four α-dN lesions on DNA replication *in vivo*, we did not analyze further the effect of local sequence context on the efficiency and fidelity of DNA replication across α-dN lesions.

We next assessed the *in vivo* replication of the α-dN lesions in SOS-induced AB1157 cells deficient in Pol II, Pol IV or Pol V and compared the results to what we observed for the isogenic wild-type AB1157 cells (Figure 5B). Depletion of Pol II led to a significant drop in the T→A mutation for α-dT. In contrast, deficiency in Pol II led to a significant increase in the C→G transversions for α-dC and the appearance of a T→G mutation that was not observed in wild-type AB1157 cells (Figure 5B). The elevation in C→G mutation in Pol II-deficient cells was accompanied by an elevated BPE for α-dC, a finding that perhaps can be attributed to the recognition of the α-dC:dC mispair by the exonuclease activity of Pol II (29,30). The absence of Pol IV only gave rise to a significant increase in C→A mutation for α-dC (Figure 5B). Removal of Pol V led to a significant decline in T→A mutation for α-dT and an abrogation of C→G mutation for α-dC. The latter finding suggests that Pol V is the major polymerase responsible for the misincorporation of dCMP and dTMP opposite α-dC and α-dT, respectively. Dual depletion of Pol IV and Pol V abolishes all the mutations observed for all the α-dNs, including the C→A (for α-dC) and T→A (for α-dT) mutations observed in cells deficient in Pol IV or Pol V alone (Figure 5B). These results indicate that the mis-insertion of dTMP opposite α-dC and α-dT depends upon both Pol IV and Pol V. Together, these results demonstrated that the effects of SOS-induced TLS polymerases on the mutagenic properties of the α-dN lesions are highly dependent on the identities of the modified nucleosides.

Proposed base-pairing interactions

The findings about the mutagenic properties of the α-dN lesions can perhaps be rationalized from the unique base-pairing properties of the nucleobases endowed by the inversion of the *N*-glycosidic bond configuration. A previous NMR solution-structure study of a duplex DNA containing an α-dA with a neighboring 3′-guanine revealed that α-dA is largely intra-helical, where the adenine base forms reverse Watson–Crick hydrogen-bonding interactions with the thymine base in the complementary strand (Scheme 2) (31). We reasoned that such reverse Watson–Crick base pairing may also occur at the active site of DNA polymerases, thereby leading to accurate and relatively efficient bypass of α-dA. The inversed *N*-glycosidic bond configuration in α-dC and α-dG may also enable their favorable base-pairing with dT through their Watson–Crick hydrogen bonding face (e.g. via reverse Wobble base pairing for the α-dG:dT mispair, Scheme 2), thereby leading to high frequencies of C→A and G→A mutations in uninduced AB1157 cells. Similar mispairing of α-dT with dT can be proposed to account for the T→A mutation found for this modified nucleoside in SOS-induced cells (Scheme 2). The differences in the effects of the different SOS-induced DNA polymerases on the four α-dN lesions may reflect their differential capacity to accommodate the mispairs formed from the various α-dN lesions at their active sites.

CONCLUSIONS

About 25 years ago, Lesiak *et al*. (11) reported the efficient formation (at a yield of 1.3–1.5%) of α-dA in isolated DNA upon exposure to 500 Gy of γ rays under anoxic conditions. The identification of the modified nucleoside was based on its co-elution with the synthetic standard of α-dA on an LC column. It remains possible that other modified nucleosides co-elute with α-dA, which would give rise to an over-estimation of the level of this modified nucleoside in DNA. Later Hwang *et al*. (10) found that, in a synthetic duplex DNA, the rate constant for the conjugation of the C1′ radical of dU with O_2 is much larger (by 2–3 orders of magnitude) than the trapping of this radical by common thiol-containing compounds, suggesting that abasic sites and strand breaks would be the primary products of C1′ radicals. Thus, it was proposed that α-dNs may not constitute an important family of DNA lesions *in vivo* (10). In the present study, we report, for the first time, the unambiguous identification of α-dG in mammalian tissue DNA. Through chemical syntheses of all three epimeric 2-deoxyribose lesions of dG and LC-MS/MS analysis, we were able to quantify the level of α-dG without the interference of the structurally similar C3′ and C4′ epimeric lesions of dG or unmodified dG. We found that α-dG is present in DNA isolated from mouse pancreatic tissues and in commercially available calf thymus DNA at substantial levels, i.e. 2.2–2.7 lesions per 10^6 nucleosides, which is approximately four-fold higher than the corresponding level of *S*-cdG. This result underscores the potential biological significance of the family of α-dN lesions. Future studies will include investigating whether the accumulation of α-dG and other α-dN lesions is tissue-specific and if it is modulated by DNA repair capacity.

We also conducted the first comprehensive study about the impact of α-dN lesions on DNA replication *in vivo*. Previously, replication studies were performed only for α-dA in wild-type *E. coli* cells (13). Here, we significantly broadened our understanding about the biological consequences of this family of under-investigated DNA lesions in terms of their impact on DNA replication using a shuttle-vector method. In doing so, we defined, for the first time, the degree to which the α-dNs block DNA replication and induce mutations in *E. coli* cells as well as the roles of SOS-induced TLS polymerases in bypassing these lesions *in vivo*. Our results showed that, in the absence of SOS induction, α-dT, α-dG and α-dC block DNA replication almost completely, with the BPEs being 1–3%, whereas α-dA constituted only a moderate block to DNA replication (with a BPE of 24%). Additionally, without SOS induction, α-dG and α-dC direct significant frequencies of dTMP mis-insertion, as manifested by 60% of G→A and 72% of C→A mutations observed for these two lesions. SOS induction significantly promotes the replication efficiency across the α-dN lesions, abolishes the mutations induced by α-dG and reduces the mutation frequency of α-dC (i.e., C→A). On the other hand, SOS induction stimulates T→A and C→G mutations for α-dT and α-dC, respectively.

Using cells deficient in Pol II, Pol IV, Pol V, or both Pol IV and Pol V, we found that misincorporation of dTMP opposite α-dT (T→A) and α-dC (C→A), and possibly subsequent extension beyond the lesion sites, requires both Pol IV and Pol V, whereas only Pol V is necessary for the mis-insertion of dCMP opposite α-dC (C→G). We also observed that Pol II reduces the misincorporation of dCMP opposite α-dC and α-dT, but promotes the insertion of the incorrect dTMP opposite α-dT.

Provided that the DNA alterations induced by the α-dN lesions are purely structural and result from inversion of configuration at the C1′-position of the 2-deoxyribose moiety, the findings made in the present study underscore the significant impact of 2-deoxyribose modifications on DNA replication *in vivo*. It will be important to examine how the α-dN lesions perturb DNA replication in mammalian cells in the future.

ACKNOWLEDGEMENT

We thank Profs John M. Essigmann and Graham C. Walker for kindly providing the initial M13 plasmid and *E. coli* cells.

SUPPLEMENTARY DATA

Supplementary Data are available at NAR Online.

FUNDING

National Institutes of Health (NIH) [R01 CA101864, P01 AG043376 and, for N.J.A., T32 ES018827]. Funding for open access charge: NIH [R01 CA101864].
Conflict of interest statement. None declared.

REFERENCES

1. Finkel,T. and Holbrook,N.J. (2000) Oxidants, oxidative stress and the biology of ageing. *Nature*, **408**, 239–247.
2. Marnett,L.J. (2000) Oxyradicals and DNA damage. *Carcinogenesis*, **21**, 361–370.
3. Dedon,P.C. (2008) The chemical toxicology of 2-deoxyribose oxidation in DNA. *Chem. Res. Toxicol.*, **21**, 206–219.
4. Amato,N.J. and Wang,Y. (2014) Epimeric 2-deoxyribose lesions: products from the improper chemical repair of 2-deoxyribose radicals. *Chem. Res. Toxicol.*, **27**, 470–479.
5. Pogozelski,W.K. and Tullius,T.D. (1998) Oxidative strand scission of nucleic acids: Routes initiated by hydrogen abstraction from the sugar moiety. *Chem. Rev.*, **98**, 1089–1108.
6. von Sonntag,C. (1987) *The Chemical Basis of Radiation Biology*. Taylor & Francis, London.
7. Bryant-Friedrich,A.C. (2010) Fate of DNA sugar radicals. In: Fishbein,JC (ed). *Advances in Molecular Toxicology*. Elsevier Science, Vol. **4**, pp. 127–155.
8. Chatgilialoglu,C., Ferreri,C., Bazzanini,R., Guerra,M., Choi,S.Y., Emanuel,C.J., Horner,J.H. and Newcomb,M. (2000) Models of DNA C1′ radicals. Structural, spectral, and chemical properties of the thyminylmethyl radical and the 2′-deoxyuridin-1′-yl radical. *J. Am. Chem. Soc.*, **122**, 9525–9533.
9. Goodman,B.K. and Greenberg,M.M. (1996) Independent generation and reactivity of 2′-deoxyurid-1′-yl. *J. Org. Chem.*, **61**, 2–3.
10. Hwang,J.T. and Greenberg,M.M. (1999) Kinetics and stereoselectivity of thiol trapping of deoxyuridin-1′-yl in biopolymers and their relationship to the formation of premutagenic α-deoxynucleotides. *J. Am. Chem. Soc.*, **121**, 4311–4315.
11. Lesiak,K.B. and Wheeler,K.T. (1990) Formation of α-deoxyadenosine in polydeoxynucleotides exposed to ionizing radiation under anoxic conditions. *Radiat. Res.*, **121**, 328–337.
12. Friedberg,E.C., Walker,G.C., Siede,W., Wood,R.D., Schultz,R.A. and Ellenberger,T. (2006) *DNA Repair and Mutagenesis*. ASM Press, Washington, D.C.

13. Shimizu,H., Yagi,R., Kimura,Y., Makino,K., Terato,H., Ohyama,Y. and Ide,H. (1997) Replication bypass and mutagenic effect of α-deoxyadenosine site-specifically incorporated into single-stranded vectors. *Nucleic Acids Res.*, **25**, 597–603.
14. Neeley,W.L., Delaney,S., Alekseyev,Y.O., Jarosz,D.F., Delaney,J.C., Walker,G.C. and Essigmann,J.M. (2007) DNA polymerase V allows bypass of toxic guanine oxidation products *in vivo*. *J. Biol. Chem.*, **282**, 12741–12748.
15. Yamaguchi,T. and Saneyoshi,M. (1984) Synthetic nucleosides and nucleotides. XXI. On the synthesis and biological evaluations of 2′-deoxy-alpha-D-ribofuranosyl nucleosides and nucleotides. *Chem. Pharm. Bull. (Tokyo)*, **32**, 1441–1450.
16. Seela,F., Heckel,M. and Rosemeyer,H. (1996) Xylose-DNA containing the four natural bases. *Helv. Chim. Acta*, **79**, 1451–1461.
17. Fox,J.J. and Miller,N.C. (1963) Nucleosides. XVI. Further studies of Anhydronucleosides. *J. Org. Chem.*, **28**, 936–941.
18. Michelson,A.M. and Todd,A.R. (1955) Deoxyribonucleosides and related compounds. Part V. cycloThymidines and other thymidine derivatives. The configuration at the glycosidic centre in thymidine. *J. Chem. Soc.*, 816–823.
19. Giese,B., Erdmann,P., Giraud,L., Gobel,T., Petretta,M., Schafer,T. and Vonraumer,M. (1994) Heterolytic C,O-bond cleavage of 4′-nucleotide radicals. *Tetrahedron Lett.*, **35**, 2683–2686.
20. Wackernagel,F., Schwitter,U. and Giese,B. (1997) Synthesis of 4′-C-phenylselenated deoxyribonucleosides by radical epimerization. *Tetrahedron Lett.*, **38**, 2657–2660.
21. Morvan,F., Rayner,B., Imbach,J.L., Thenet,S., Bertrand,J.R., Paoletti,J., Malvy,C. and Paoletti,C. (1987) α-DNA II. Synthesis of unnatural α-anomeric oligodeoxyribonucleotides containing the four usual bases and study of their substrate activities for nucleases. *Nucleic Acids Res.*, **15**, 3421–3437.
22. Delaney,J.C. and Essigmann,J.M. (2006) Assays for determining lesion bypass efficiency and mutagenicity of site-specific DNA lesions *in vivo*. *Methods Enzymol.*, **408**, 1–15.
23. Zhai,Q., Wang,P., Cai,Q. and Wang,Y. (2014) Syntheses and characterizations of the *in vivo* replicative bypass and mutagenic properties of the minor-groove O^2-alkylthymidine lesions. *Nucleic Acids Res.*, **42**, 10529–10537.
24. Delaney,J.C. and Essigmann,J.M. (2004) Mutagenesis, genotoxicity, and repair of 1-methyladenine, 3-alkylcytosines, 1-methylguanine, and 3-methylthymine in *alkB Escherichia coli*. *Proc. Natl. Acad. Sci. U.S.A.*, **101**, 14051–14056.
25. Yuan,B., Cao,H., Jiang,Y., Hong,H. and Wang,Y. (2008) Efficient and accurate bypass of N^2-(1-carboxyethyl)-2′-deoxyguanosine by DinB DNA polymerase *in vitro* and *in vivo*. *Proc. Natl. Acad. Sci. U.S.A.*, **105**, 8679–8684.
26. Zhai,Q., Wang,P. and Wang,Y. (2014) Cytotoxic and mutagenic properties of regioisomeric O^2-, N3- and O^4-ethylthymidines in bacterial cells. *Carcinogenesis*, **35**, 2002–2006.
27. Jaruga,P. and Dizdaroglu,M. (2008) 8,5′-Cyclopurine-2′-deoxynucleosides in DNA: mechanisms of formation, measurement, repair and biological effects. *DNA Repair*, **7**, 1413–1425.
28. Wang,J., Yuan,B., Guerrero,C., Bahde,R., Gupta,S. and Wang,Y. (2011) Quantification of oxidative DNA lesions in tissues of Long-Evans Cinnamon rats by capillary high-performance liquid chromatography-tandem mass spectrometry coupled with stable isotope-dilution method. *Anal. Chem.*, **83**, 2201–2209.
29. Cai,H., Yu,H., McEntee,K., Kunkel,T.A. and Goodman,M.F. (1995) Purification and properties of wild-type and exonuclease-deficient DNA polymerase II from *Escherichia coli*. *J. Biol. Chem.*, **270**, 15327–15335.
30. Vaisman,A., McDonald,J.P. and Woodgate,R. (2012) Translesion DNA synthesis. *Ecosal Plus*, doi:10.1128/ecosalplus.7.2.2.
31. Johnson,C.N., Spring,A.M., Desai,S., Cunningham,R.P. and Germann,M.W. (2012) DNA sequence context conceals α-anomeric lesions. *J. Mol. Biol.*, **416**, 425–437.
32. Guerrero,C.R., Wang,J. and Wang,Y. (2013) Induction of 8,5′-cyclo-2′-deoxyadenosine and 8,5′-cyclo-2′-deoxyguanosine in isolated DNA by Fenton-type reagents. *Chem. Res. Toxicol.*, **26**, 1361–1366.